catalysts

MDPI

Article

Synthesis and Evaluation of Copper-Supported Titanium Oxide Nanotubes as Electrocatalyst for the Electrochemical Reduction of Carbon Oxide to Organics

SK Safdar Hossain [1,*], Junaid Saleem [2], SleemUr Rahman [3], Syed Mohammed Javaid Zaidi [4], Gordon McKay [2] and Chin Kui Cheng [5]

1 Department of Chemical Engineering, College of Engineering, King Faisal University, Hofuf-31982, Saudi Arabia
2 Division of Sustainable Development, College of Science & Engineering, Hamad Bin Khalifa University, Qatar Foundation, Doha, Qatar; jsaleem@hbku.edu.qa (J.S.); gmckay@hbku.edu.qa (G.M.)
3 Chemical Engineering Department, King Fahd University of Petroleum & Minerals, Dhahran-31261, Saudi Arabia; sleemur@midadholdings.com
4 Center for Advanced Materials, Qatar University, Doha, Qatar; smjavaidzaidi@gmail.com
5 Faculty of Chemical and Natural Resources Engineering, Universiti Malaysia Pahang, Lebuhraya Tun Razak, Kuantan 26300, Pahang, Malaysia; Chinkui@ump.edu.my
* Correspondence: snooruddin@kfu.edu.sa

Received: 30 January 2019; Accepted: 18 March 2019; Published: 25 March 2019

Abstract: Carbon dioxide (CO_2) is considered as the prime reason for the global warming effect and one of the useful ways to transform it into an array of valuable products is through electrochemical reduction of CO_2 (ERC). This process requires an efficient electrocatalyst with high faradaic efficiency at low overpotential and enhanced reaction rate. Herein, we report an innovative way of reducing CO_2 using copper-metal supported on titanium oxide nanotubes (TNT) electrocatalysts. The TNT support material was synthesized using alkaline hydrothermal process with Degussa (P-25) as a starting material. Copper nanoparticles were anchored on the TNT by homogeneous deposition-precipitation method (HDP) with urea as precipitating agent. The prepared catalysts were tested in a home-made H-cell with 0.5 M $NaHCO_3$ aqueous solution in order to examine their activity for ERC and the optimum copper loading. Continuous gas-phase ERC was carried out in a solid polymer electrolyte (SPE) reactor. The 10% Cu/TNT catalysts were employed in the gas diffusion layer (GDL) on the cathode side with Pt-Ru/C on the anode side. Faradaic efficiencies for the three major products namely methanol, methane, and CO were found to be 4%, 3%, and 10%, respectively at −2.5 V with an overall current density of 120 mA/cm^2. The addition of TNT significantly increased the catalytic activity of electrocatalyst for ERC. It is mainly attributed to their better stability towards oxidation, increased CO_2 adsorption capacity and stabilization of the reaction intermediate, layered titanates, and larger surface area (400 m^2/g) as compared with other support materials. Considering the low cost of TNT, it is anticipated that TNT support electrocatalyst for ECR will gain popularity.

Keywords: electrochemical reduction; carbon dioxide; titanium oxide nanotubes; Cu nanoparticles

1. Introduction

It has been scientifically well established that carbon dioxide (CO_2), a major greenhouse gas, is the prime reason for the climate change and global warming phenomena in recent decades [1,2]. A substantial share of the anthropological CO_2 comes from coal and natural gas-fired power plants,

combustion of liquid fuels in automobiles, and other industrial activities [3–5]. Renewable sources of energy (solar, wind) with suitable energy storage devices (batteries, supercapacitors, and fuel cells) have been increasingly adopted to limit the CO_2 generation [6–8]. Many processes such as photochemical and electrochemical reduction, (CO_2) dry reforming of methane have been devised to chemically convert CO_2 into high economic value products such as, methanol, ethanol, formic acid, synthesis gas, methane, and ethylene, which are traditionally obtained from fossil fuels [3,9–11]. Electrochemical reduction of CO_2 is an elegant method to transform CO_2 into an array of valuable products with many attractive features [12]. This process takes place in an electrochemical reactor where the reduction of CO_2 takes place at the cathode and water oxidation takes place at the anode using electrical energy from a conventional grid or renewable source [13–15]. The main advantages of electrochemical reduction of CO_2 (ERC) are the requirement of benign process condition (room temperature and atmospheric pressure) and tunable product distribution using different cathode materials [16,17]. Moreover, in the near future, a steady supply of nearly pure and low-cost CO_2 will be available from the CO_2 storage and underground sequestration (CSS) plants [18]. However, there are some practical challenges for the large-scale utilization of the ERC process which include large over potentials for the hydrocarbon product(s), low overall current density, and small faradaic efficiency for the desired product(s) [19,20]. Since the early work of Hori et al. in 1986 [21], most of the transition (metal and oxides), and noble metals have been explored as the cathode material in aqueous, organic, and ionic liquid medium [22]. However, the solubility of CO_2 in water or non-aqueous medium remains poor at room temperatures and product selectivity is also low because at the high potential range competing hydrogen evolution reaction (HER) predominates [23]. Hence, for ERC to become economically viable, it is indispensable to develop non-precious metal electrocatalyst which offers low over potential and high current density for the CO_2 reduction reaction and high faradaic efficiency for the desired product(s) by increasing the overpotential for the HER [23].

Copper is perhaps the most explored electrode material for the ERC. It is the only metal that has been reported to form lower hydrocarbons (methane and ethylene), alcohols (methanol, ethanol, and propanol), formate, and carbon monoxide with reasonable current density and faradaic efficiency [20,24]. Copper shows low hydrogen overpotential and adsorption of CO which leads to more reduced products such as, methanol, and lower hydrocarbons [25–27]. Copper has been employed as an electrode in various forms such as bulk metal [28,29], suspended copper particles [30], oxides of copper [31–34], copper nano particles [26], copper nanowires [27], and copper nanocubes [35]. The overall performance of the electrode depends on the physical nature (roughness, thickness, porosity) and chemical (oxidation states, facet, grain boundary, and polycrystallinity) of the Cu electrodes.

It is well established that dispersing metals on high surface area, and electrically conducting support materials leads to better utilization of precious metals, lower metal loadings, improved activity, and stability in electrochemical reactions. Many carbonaceous support materials such as activated carbon [36], carbon nanubes [37,38], graphenes [39], metal-organic frameworks [19,40], and mesoporous carbon [41] have been explored recently as support material for ERC. Carbon-based support materials experience corrosion at operating potentials above ~1 V which can lead to fast deactivation of the catalysts due to loss of active metal sites and metal agglomeration [42]. Titanium oxide (TiO_2) has generated lots of interests as a support material for the electrochemical applications, including ERC, due to its unique physical and chemical properties, excellent metal support interaction, excellent stability in the alkaline and acidic environment, and low cost [10,43,44]. Titanium oxide has been reported as support materials for borohydride oxidation [45], direct methanol fuel cells [46,47], and direct formic acid fuel cells [48] Cueto et al. studied the electrochemical reduction of CO_2 on electrodeposited nanosized (250 nm) Ag particles on a thin film titanium oxide electrode to understand the kinetics of ERC [49]. Ma et al. extensively investigated the ERC in a flow reactor and in aqueous 0.5 M K_2SO_4 solution standard H-cell to understand the role of TiO_2 as support material and the effect of Ag loading and particle size on the performance of Ag/TiO_2 catalyst for the conversion CO_2 to CO. They were able to produce CO with faradaic efficiency higher than 90% at partial current

density 101 mA/cm^2 with 40 wt.% Ag/TiO_2 which is two times higher than 40% Ag/C. The beneficial effect of TiO_2 originates from its ability to promote the formation of small (~10 nm), well dispersed Ag nanoparticles, increased CO_2 adsorption capacity, stabilization of the intermediate and it also serves as redox electro carrier [50]. Yuan et al. carried out electro-reduction of CO_2 over high copper loading up to 80% on titanium oxide. Among various composition, 40% Cu/TiO_2 showed highest faradaic efficiency of 27.4% for the ethanol formation. Trace amounts of methanol and propanol was also detected in products. The catalysts showed excellent activity as well as enhanced stability where current density of 8.66 mA/cm^2 was maintained for more than 25 h of continuous performance. The excellent activity was attributed to the synergic interaction between Cu and TiO_2 nanoparticles arising from strong metal support interaction [51]. In similar work, CuO supported on TiO_2 was thoroughly investigated for the ERC by Yuan et al. Ethanol, acetone, and n-propanol were detected with an overall faradaic efficiency of 47.4% [52]. Better catalytic activity was associated with the large electrochemical surface area and good CO_2 adsorption capacity. Titanium oxides nanotubes (TNT) are an interesting structural form of TiO_2. Titanium oxide nanotubes could provide extra features of the tubular structure while retaining the advantage of TiO_2, that facilitates the charge transfer during the electrochemical reaction and the high porous structure allows easier transport of adsorbed intermediates to enhance the reaction rate. Qu et al. investigated the RuO2 loaded on TNT as a potential electrocatalyst in 0.5 M $NaHCO_3$ solution. They reported 60.5% faradic efficiency for methanol in the aqueous phase. High activity was attributed to the unique tubular structure [53].

Most of the studies reported so far on ERC has traditionally been conducted in standard three-cell electrodes in an aqueous or non-aqueous medium as the electrolyte at low current densities. The focus has been on studying the fundamental aspects of kinetics and mechanism of the electrochemical reduction on various electrode surfaces. However, for the ERC process to be economically viable for commercialization, the reaction should be carried out in a continuous flow reactor at high current densities (~200 mA/cm^2) and in the gas phase to overcome the mass transfer issue originating from the limited solubility of CO_2 in aqueous and non-aqueous mediums [54,55]. Dewulf et al. carried out ERC at the copper-coated Nafion 115 as solid polymer electrode to produce methane and ethylene with the faradaic efficiency of more than 20% at room temperature [56]. Komatsu et al. reported a faradaic efficiency of 19% for the major product, ethylene, at −1.7 V vs. SCE on solid polymer electrolyte (SPE) prepared by coating copper on Nafion 117 membrane, while formic acid and CO were found to be the major products in case of an anion exchange membrane SPE (Selemion AMV) [57]. Delacourt et al. used a set up similar to the polymer electrolyte membrane fuel cell to produce syngas (CO + H_2) using unsupported Ag nanoparticles or Ag/C as a cathode catalyst. They introduced the concept of adding a buffer layer of glass fiber soaked $NaCHO_3$ to improve faradaic efficiency. They produced CO with the efficiency of 82% and H_2 efficiency of 10–15% [54,58]. Recently, Basu et al. reported an overall faradaic efficiency of 39.6% for methane, methanol, and ethane as the major product in the ERC on gas phase reaction over copper nanoparticles [26].

To the best of the authors' knowledge, copper supported on TNT has never been studied as a catalyst for ERC in a continuous gas phase solid polymer electrolyte reactor. In this work, we report the ERC over Cu/TNT electrocatalysts containing different copper loadings (5%, 10%, and 20% by wt.) in the aqueous sodium bicarbonate solution and in a continuous gas-phase SPE reactor.

2. Results and Discussion

2.1. XRD

X-ray diffraction (XRD) spectrum for the TNT samples with and without copper loading onto TNT are shown in Figure 1. X-ray diffraction was carried out to investigate the different phases present in the samples and to calculate the crystallite size of the phases. For the pristine TNT, prominent diffraction peaks at 2θ angles of 24.8°, 37.4°, 47.8°, 53.5°, 55.3°, and 62.2° were observed. These diffractions peaks could be assigned to the (101), (004), 200), (105), (211), and (204) crystal planes, respectively, of the

tetragonal anatase phase (JCPDS Card no. 21-1272) [59,60]. The two diffraction peaks at 2θ angles of 27.4° and 36.3° correspond to the spacing of (1 1 0) and (1 0 1), respectively, of the rutile phase (JCPDS Card no. 21-1276) [59]. Here, the rutile content of the TNT was very small compared to the anatase. It is generally known that in the hydrothermal synthesis of TNT, the heat treatment above 800 °C or acid hydrothermal processes lead to the formation of rutile phase [60–62]. It is also possible that some of the diffraction peaks of rutile phase TiO_2 may not appear in the XRD pattern because the nanotubes may be formed by the rolling up the two-dimensional sheets of TiO_2 structure [63]. The effect of copper loading on the TNT is depicted by the XRD spectra in Figure 1. From the XRD pattern for 5% Cu deposited on TNT, it is evident that only copper oxide peak at 35.48° was visible, which corresponds to phase (111) (JCPDS-050667). The crystallite size of the copper oxide was calculated using Scherer equation, which was found to be 7.6 nm. The crystallite size plays important role in the catalytic activity of the catalyst. At lower copper loadings, the small intensity of the peaks related to copper metals may be due to the formation of Cu nanoparticles of highly dispersed and very small crystal size. It could also be due to the absence of enough Cu material to form crystals [64]. It is to be noted that peaks associated with anatase phase remained unchanged even after the copper loading. A similar peak was found for 10% copper loading with crystallite size 2.2 nm. For 20% Cu on TNT, apart from the anatase peaks, strong diffractions peaks appeared at 43.2°, 50.2°, and 73 ° which can be ascribed to the (111), (200), and (220) planes of the copper in metallic phase (Cu°) (JCPDS Card no. 85-1326) [65,66]. It shows that the CuO oxide, generated as a result of a deposition-precipitation process and subsequent calcination at 450 °C in presence of Ar gas, was mostly reduced to the copper in the metallic state by the 5% H_2 in Argon. The crystallite size for the Cu (111) was calculated to be 18 nm. Therefore, it is concluded that nanosized copper particles were successfully deposited on TNT keeping the original structure of the TNT intact.

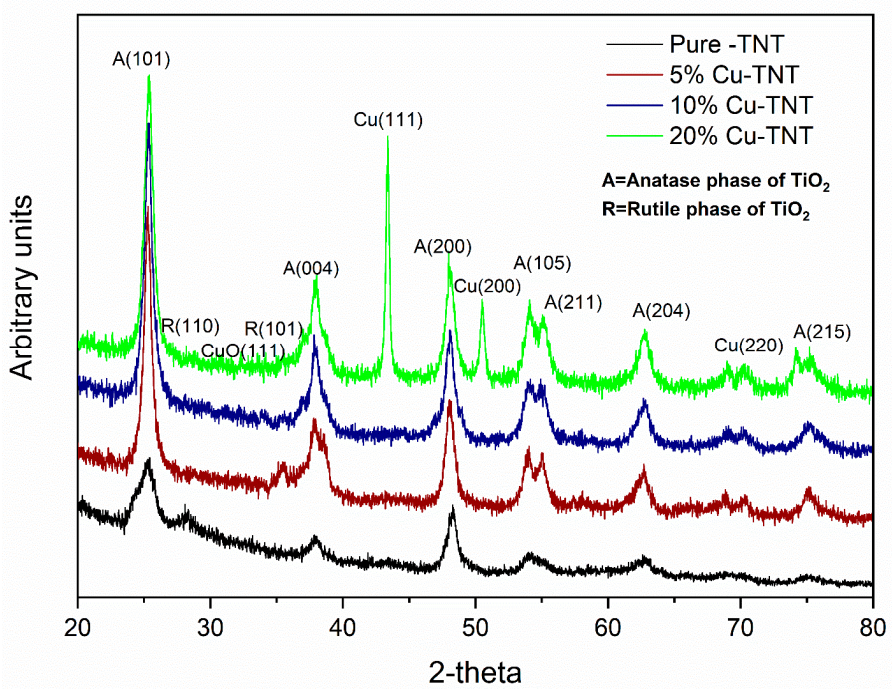

Figure 1. XRD spectra for the prepared catalysts.

2.2. SEM-EDX

Tube-like structure of titanium oxide was obtained by the alkaline hydrothermal method followed by calcination. The structure and morphology of pristine TNT and copper loaded TNT were ascertained using SEM, while EDX was used to identify and measure the "surface" composition of the catalysts. Figure 2A,B shows the SEM image of the pristine TNT. The tube-like structure was obvious from the

Figure 2B with lots of empty spaces. This shows the successful preparation of tube-like structure. When copper was deposited, the metal was deposited on the surface of the TNT. As the loading of copper increased, the empty spaces started to be filled up with copper metal and agglomerations were visible. However, the original structure remained intact even after the deposition of Copper. Figure 2C shows the EDX spectrum for the 20% Cu/TNT that clearly shows the peaks associated with Cu, Ti, and O in the samples. The unlabeled peaks found in the 0.8–2.4 keV range is due to the aluminum holder used for holding the sample. The composition of the catalysts is summarized in Table 1. It further shows that the catalyst composition can be precisely controlled by the homogenous precipitation-deposition method.

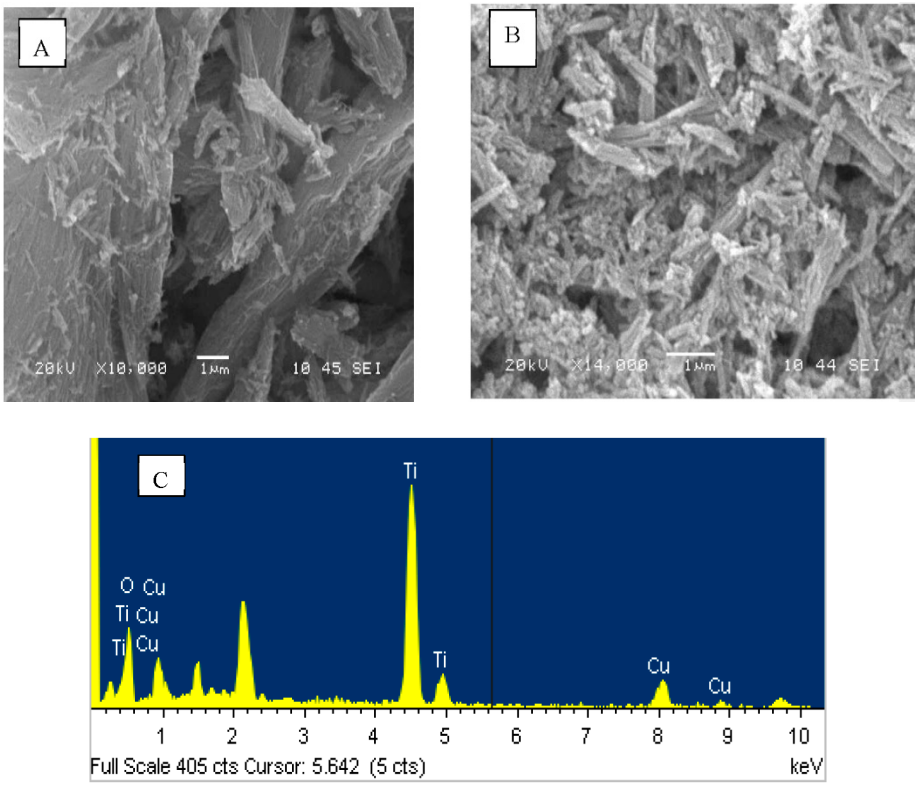

Figure 2. (**A**,**B**) SEM images of pure titanium oxides nanotubes (TNT) and for 20% Cu/TNT electrocatalysts (**C**) EDX spectrum for 20% Cu/TNT electrocatalysts.

Table 1. BET surface area and chemical composition.

Catalysts	BET Surface Area (m^2/g)	Pore Volume (cm^3/g)	Cu (wt.%)	Ti (wt.%)	O (wt.%)
Degussa (P-25)	56.86	0.20	-	49.6	50.4
TNT	323.53	0.84	-	49.6	50.4
5% Cu/TNT	258.2	0.67	4.6	53.3	42.1
10% Cu/TNT	190.2	0.51	10.79	50.62	38.59
20% Cu/TNT	87.77	0.39	16.3	46.4	37.2

2.3. TEM

Transmission electron microscope (TEM) analysis was carried out to study the detailed morphology of the prepared catalysts. Figure 3A shows the nearly spherical nanoparticles of 20 nm average particle size that were present in the starting material, titanium oxide. Figure 3B–D show the TEM images of the TNT and copper supported TNT catalysts. It is evident from Figure 3B that well-developed and distinct nanotubes of 5–8 nm diameter and 180–200 nm length were formed as a result of the alkaline hydrothermal process followed by calcination at 400 °C in presence of air. The spherical titanium oxide particles present in the starting material were fully transformed into

the tubular structure of TNT as a result of the alkaline treatment and calcination. It is also worth mentioning that calcination at 400 °C did not alter the otherwise tubular structure of titanium oxide nanotubes (Figure 3C). It is established in the literature that the morphology of the TNT depends on the choice of the starting material [67]. Titanium oxide in the anatase form or a mixture of rutile and anatase such as Degussa (P-25) generally favors the formation of well-defined nanotubes, which is also confirmed from this work [63]. Figure 3C shows the TEM image for 5% Cu loaded TNT. Most of Cu particles were located on the external surface of the TNT without incorporating clusters into the pores of TNT. It is evident that spherical metal particles were well distributed on the surface of the TNT and their mean particle size is 10 nm. Figure 3D,E shows the TEM images for 20% Cu/TNT. It can be seen that the tubular structure of the TNT was mostly covered with the copper particles at higher loading.

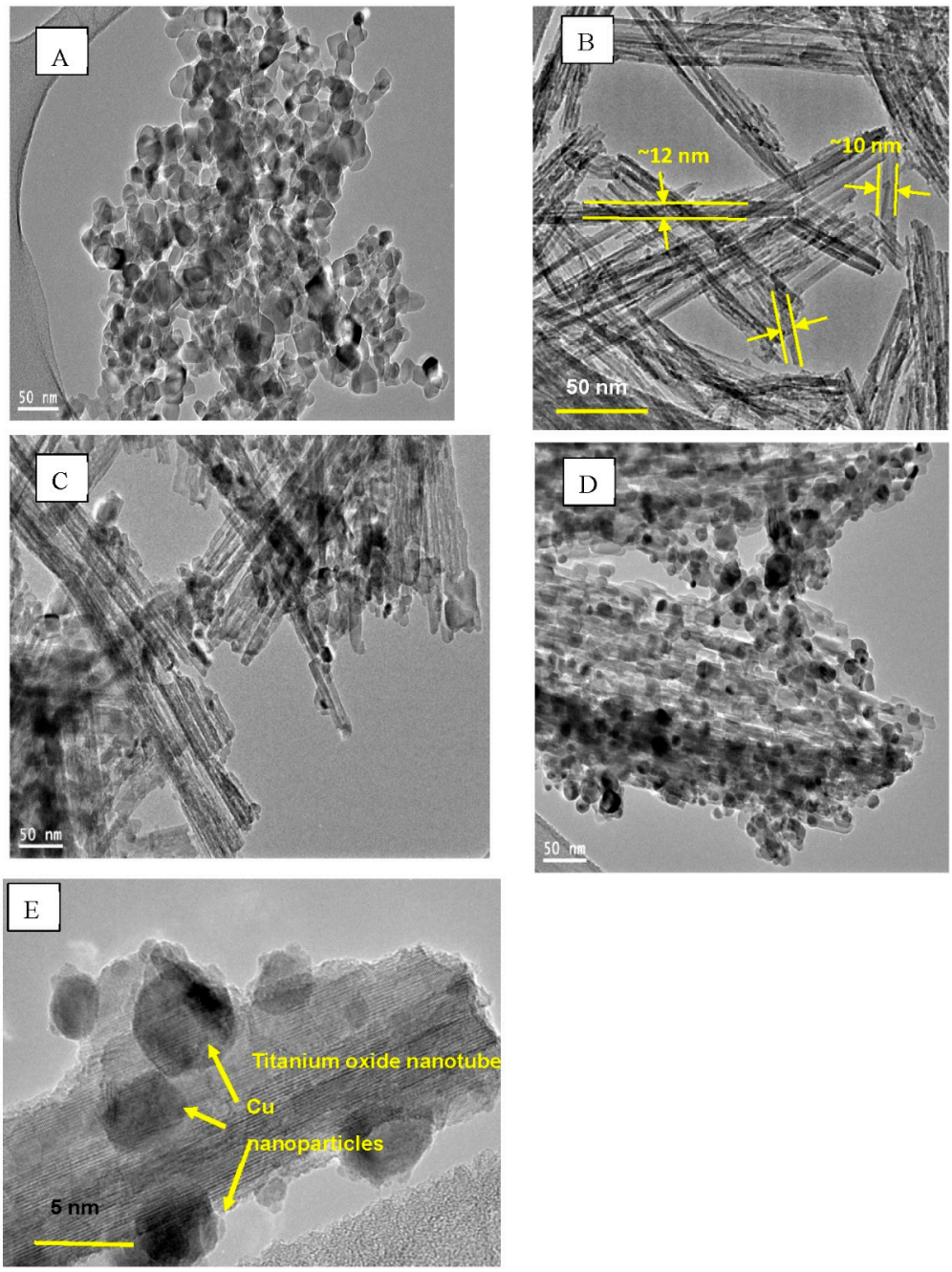

Figure 3. TEM images for (**A**) Degussa (P-25), (**B**) pristine TNT, (**C**) 5% Cu/TNT, (**D**) 20% Cu/TNT, and (**E**) high-resolution TEM image for 20% Cu/TNT.

2.4. Nitrogen Adsorption–Desorption Isotherms

The Brunauer-Emmett-Teller (BET) surface area, pore volume, and pore size of the support material and the copper supported catalysts are determined by N_2 adsorption–desorption experiments. The isotherms for Degussa, TNT support, and 20% Cu/TNT are shown in Figure 4. The results of calculations are summarized in Table 1. The surface area and pore volume of the starting material Degussa (P-25) were found to be 55.86 m^2/g and 0.2 m^3/g, respectively whereas the surface area and pore volume of titanium oxide nanotubes were 323.53 m^2/g and 0.8 m^3/g. It is apparent that the alkaline treatment and calcination led to a tremendous increase in the surface area and pore volume. Formation of a very loosely contacted structure agglomeration with large empty intertubular spaces could be the reason for the large surface area and pore volume [64,68]. Both the pore volume and surface area decreased upon incorporation of Cu through homogenous precipitation-deposition method. The surface area and pore volume for 20% Cu/TNT were found to be 87.77 m^2/g and 0.39 m^3/g.

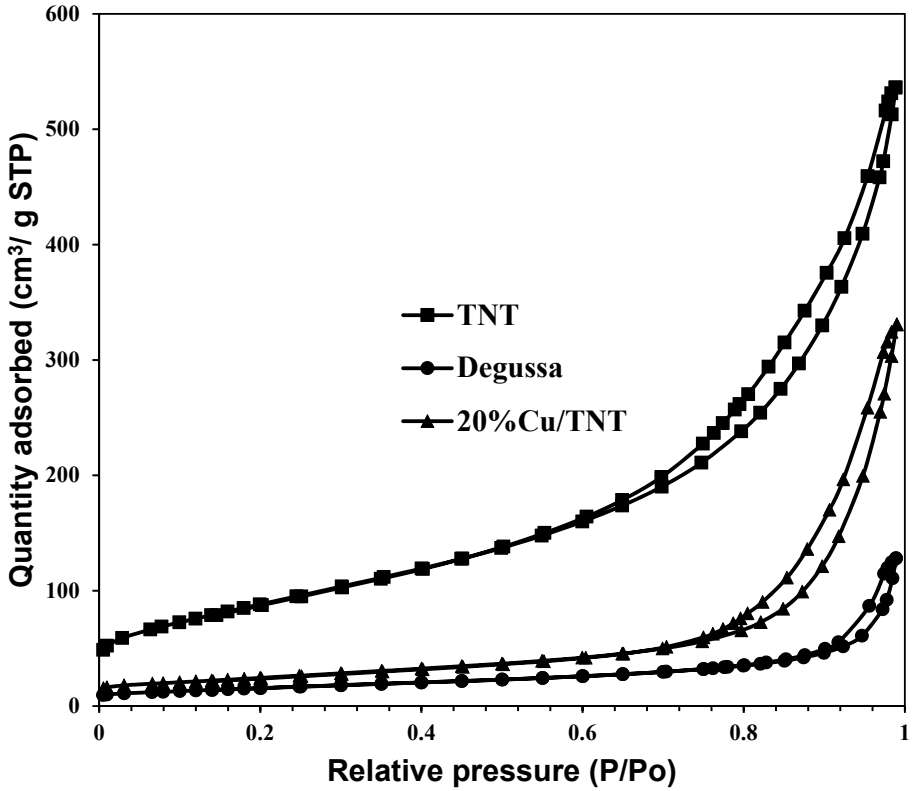

Figure 4. Nitrogen adsorption–desorption isotherms at 77 K for Degussa (P-25), TNT, and 20% Cu/TNT.

3. Electrochemical Measurements

3.1. Linear Sweep Voltammetry (LSV)

The electrocatalytic activity of the prepared catalysts for the electrochemical reduction of CO_2 were evaluated using LSV electrochemical technique in a standard electrochemical cell described in the experimental section. Pristine and TNT loaded with various amount of Cu (5, 10, and 20 wt.%) were tested for ERC in an aqueous 0.5 M $NaHCO_3$ solution saturated with CO_2. The objective was to evaluate the optimum copper loading on the TNT for the electrochemical reduction of CO_2. It is established that the supporting bicarbonate solution increases the ionic mobility thereby increasing CO_2 solubility, as well as discourages the H_2 evolution reaction [26,69]. Figure 5 shows the LSV curves for the prepared catalysts including the pristine TNT in the applied potential range of 0 to −3 V vs. SCE. The electrocatalyst samples with high catalytic activity for the ERC show high current density in

LSV in CO_2 saturated sodium bicarbonate solution. Thus, the current density in the given potential range can be used to compare the activity of the catalysts.

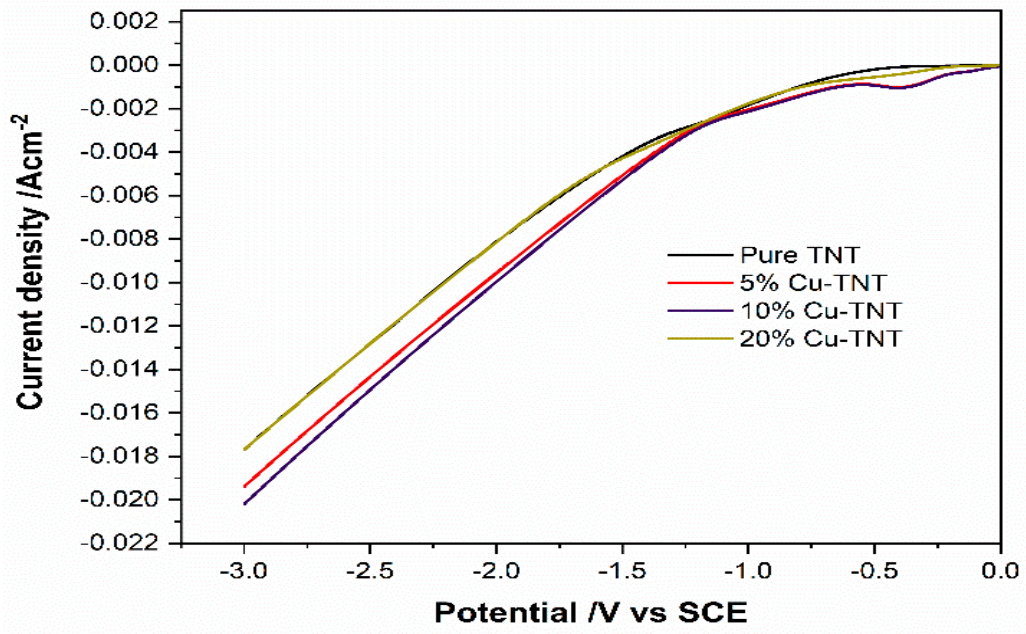

Figure 5. Linear sweep voltammetry for the prepared catalysts in aqueous 0.5 $NaHCO_3$.

It is well known that in the electrochemical processes, two competing reactions take place; the hydrogen evolution reactions (HER) and electrochemical reduction reaction of CO_2. The HER becomes more active at higher potentials. Therefore, electrochemical cells are not operated at a very high potential at which mostly the HER takes place and the contribution from the ERC becomes negligible. Unfortunately, the ERC takes place at more negative potentials than required by the equilibrium, and this increase in the potential is known as over potential. As TNT is not a very good conductor of electricity, the ionic conductivity is imparted by electrolyte solution and Nafion® ionomer during the preparation of the catalyst coated electrode. It is required that the metal particles are well in electrical contact with the working electrode as well as with the electrolyte. Figure 5 shows that the current density increased slightly with adding 5% Cu metals and further the highest current is obtained for 10% Cu loading. The current density was found to decrease with further increase in the Cu loading to 20%. For example, the current density for 10% and 20% Cu loading on TNT at −1.5 V are 0.0055 and 0.004 A /cm^2, respectively. Current densities are comparable with the current densities reported in the literature. For example, Chang et al. reported a current density of 5.57 mA/cm^2 (0.00557 A/cm^2) for Cu_2O coated carbon cloth [33]. Recently, Rasul et al. carried out an electrochemical reduction in 0.5 M $KHCO_3$ solution over oxide derived Sn–Pb–Sb and Cu–Sn alloy electrode surfaces. The current densities were found to be in the range of 7–10 mA/cm^2 (0.007–0.01 A/cm^2) [70]. A similar range of current densities is reported by Lui et al. [71]. This observation is consistent with the physical characterization results explained in the earlier sections. Titanium oxide nanotubes as support material have several advantages over the conventional support material such as activated carbon. Titanium oxide nanotubes are very stable towards oxidation, are semiconductor in nature, have layered titanates, and have large surface area. Bhattacharya et al. studied the photochemical reduction of CO_2 over the titania nanotubes and platinized titania nanotubes using FTIR. It was suggested that the Lewis acid and base sites generated on the periphery of the TNT increases the adsorption of CO_2 on the surface of the TNT [72]. Further mechanistic studies should be conducted to understand the exact nature of the enhancement mechanism in the ERC. Several theories are invoked here to explain the LSV results. At lower metal loading (say 5%), not enough metal nanoparticle active sites are present to make crystals and to catalyze the ERC effectively. However, at very high metal loading (20 wt.%

or more), the catalyst shows excessive agglomeration of copper nanoparticles, as shown in the TEM micrographs. In addition, the pores present in the pristine TNT are blocked at higher metal loading which leads to the decrease in pore volume and BET surface area (Table 1). As a result, the catalysts behave like bulk copper metal at high metal loading. These effects result in a decrease of reduction current at higher metal loading. This type of behavior is very common in catalysis [73,74]. For example, Basu et al. [73] prepared Sn/ZSM and Sn/ γ-Al_2O_3 catalysts to act as electrocatalyst for the ECR. The optimum metal loading was found to be 20% due to optimum loadings reaching to percolation limit and blocking of pores at higher loadings. It was also suggested that the percolation limit could be different for different support materials. In the case of TNT, the percolation limit is apparent between 10% and 20% metal loading. Therefore, it can be concluded that the catalysts with 10% Cu loading provide sufficient active metal site concentration, as well as a high surface area of the support which results in high current density in LSV experiments.

The electrocatalytic activity of the Cu/TNT catalysts in presence of nitrogen and carbon dioxide were confirmed by the carrying out LSV scans of 10% Cu/TNT in CO_2 saturated and N_2 saturated 0.5 M $NaHCO_3$. The LSV curves are presented in Figure 6. The difference in reduction current density in the two curves, especially at lower potentials, arose from the current density from the electrochemical reduction of CO_2. Two competing reactions, HER and ERC, took place on the Cu/TNT in aqueous 0.5 M $NaHCO_3$ solution saturated with CO_2. However, under the N_2 purged condition (in absence of CO_2) all the current density was solely due to HER. This shows that Cu/TNT is active for the ERC [37,75]. The onset potential of the ERC measured here is more positive than −1.0 vs. SCE [33,76]

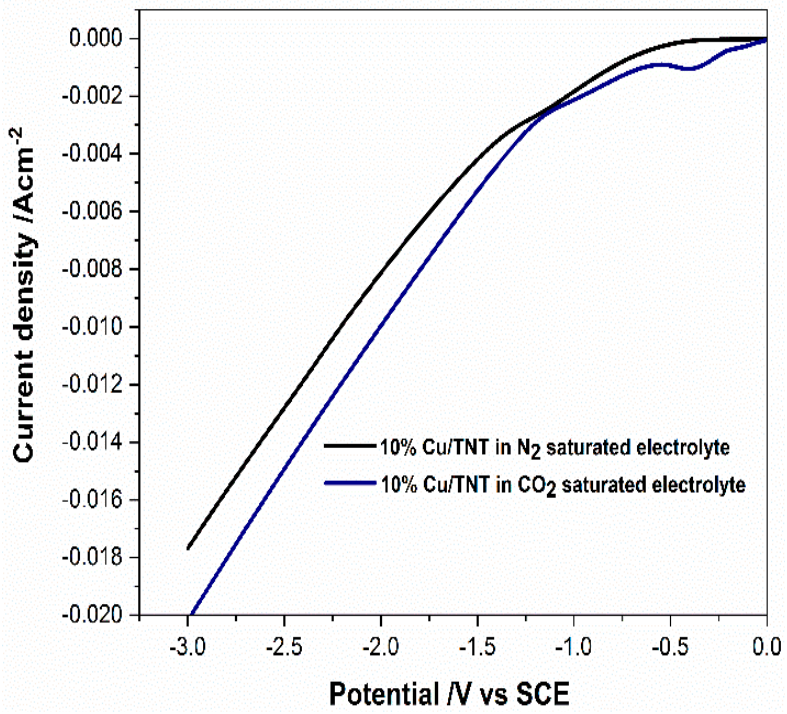

Figure 6. Linear sweep voltammetry for 10% Cu/TNT in the presence of N_2 and CO_2 saturated aqueous 0.5 $NaHCO_3$.

3.2. Chronoamperometry (CA)

Apart from the activity test, a long-term performance test of the prepared catalysts was conducted by doing chronoamperometry analysis at −1.7 V for 100 min. The rationale behind using −1.7 V is that voltages over this may produce hydrogen overwhelmingly [25]. Figure 7 shows the chronoamperometry results for the electrocatalysts [33,76–79]. It can be observed that the catalysts were stable at the potential for 100 min. Trends for chronoamperometry results were in accordance with LSV results.

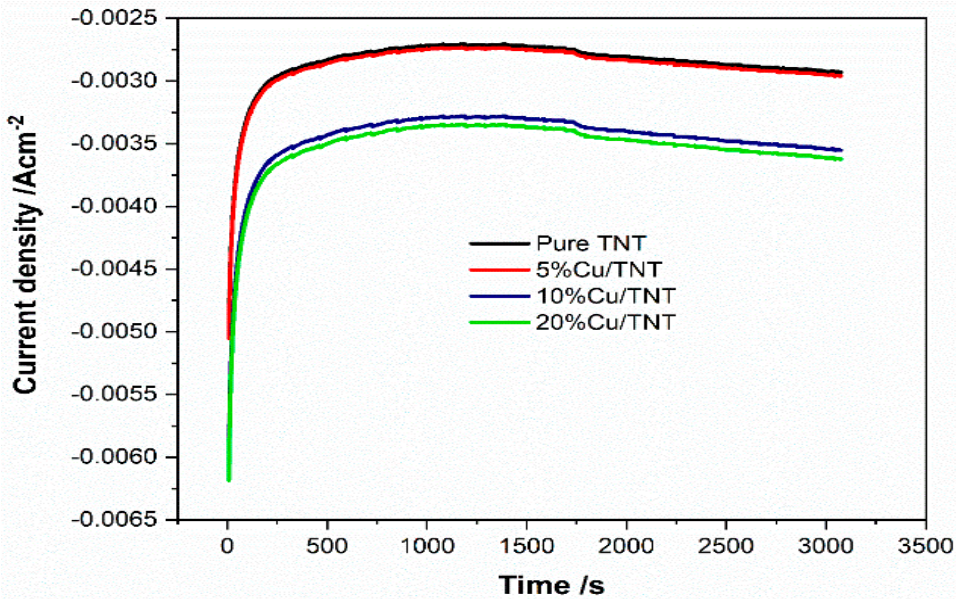

Figure 7. Chronoamperometry of the prepared catalysts at −1.7 V vs. SCE.

4. Fuel Cell Results

Electrochemical reduction of CO_2 was carried out in a continuous electrochemical reactor. The experimental setup is described in the experimental setup section. The solid polymer electrolyte membrane-based reactor uses 10% Cu/TNT as cathode and Pt-Ru/C as anode catalysts. The product analysis was carried out for the applied potentials −0.5, −1.5, −2.5, a −3.5 V with NHE as a reference potential. The gaseous products were collected in a Tedlar® gas sampling bag and analyzed using a GC. The detailed procedure to calculate the faradaic efficiency from composition data is similar to our previous paper [37]. The faradaic efficiency of the reduction products at different applied potentials is presented in Figure 8. Methanol, methane, CO, and H_2 are formed as major reduced products as a result of the electrochemical reduction of CO_2. Moreover, results show that the product distribution and their faradaic efficiency markedly change with the change in the applied potential. It is important to note that some of the C2+ organics have been missed during sample collection procedure and in the headspace of the GC-FID detector. Therefore, the total faradaic efficiency may not be summed to 100%. Most of the reported researches have focused on the electrochemical reduction of CO_2 in the liquid phase in a half cell, whereas there are very few reports on continuous fuel cell like polymeric electrolyte membrane (PEM) electrochemical reactor. Yamamato [36] carried out the ERC on Cu/ACF electrocatalyst as gas diffusion electrode in a 0.5 M $NaHCO_3$ solution. Hydrogen was the major product along with trace amount of methane. Yamamoto et al. [80] also reported the electrochemical reduction of CO_2 over Ni/ACF in a fuel cell PEM electrochemical reactor with CO and H_2 as the major product. The faradaic efficiency for CO and H_2 was 78% and 15%, respectively, at −1.9 V vs. SCE. Our group reported the production of CO and H_2, syngas, from CO_2 on NiO/MWCNT. It was concluded that the CO and H_2 ratio in syngas could be adjusted using appropriate applied potential [37]. Delarcourt et al. reported excellent faradaic efficiency, 90% for CO at 80 mA/cm^2 for CO_2 reduction over Ag/C based Nafion membrane cathode for the gas diffusion layer with $KHCO_3$ saturated buffer layer in a continuous electrolysis cell [54]. Garg et al. carried out electrochemical reduction of CO_2 in gas phase continuous reactor similar to Delarcourt et al. with Nafion as solid electrolyte, and copper nanoparticles and Pt/C as cathode and anode, respectively. Methanol and methane were reported to be the major products with an overall faradic efficiency to 39.6% [26]. A large number of CO_2 reduction products were identified on copper foil electrodes, with methane, CO, and hydrogen among the major products. The faradaic efficiency for methane was estimated to be approximately 40% at −1.2 V [81]. Basu et al. [73] have recently published a report of the ERC on Sn/ZSM and Sn/γ-Al_2O_3

in the continuous electrochemical cell. They reported CO, H_2, and methane as a major reduction product at −2 V with 20.4% as the faradaic efficiency for methane. In this work, the faradic efficiency for methanol slightly increased from 2% to 4% when the applied potential was increased from −1.5 to −2.5 V. With further increase in the potential, the faradaic efficiency for methanol decreased. Methane was produced in very small quantity. A trend similar to the faradaic efficiency for methanol was observed for the faradaic efficiency for CH_4. The faradaic efficiency for CO increased to approximately 10% when the applied potential was increased from −1.5 to −2.5 V. The highest faradaic efficiency for methanol and CO were observed at −2.5 V with a current density of 120 mA/cm^2. It is also worth noting that hydrogen was produced at all non-zero potentials. The origin of hydrogen gas was the hydrogen evolution reaction, which involved electrolysis of water. It was seen that faradaic efficiency for hydrogen increased steadily with the increase in applied potential. Hydrogen was produced at higher potentials at the expense of the products from the electrochemical reduction of CO_2. A quantitative comparison of results obtained in this work with some representative published works on supported electrocatalysts for ERC is presented in Table 2. It is evident that our results are comparable with the reported studies. However, the low total faradaic efficiency could be due to the ohmic losses in the cell, failure to identify all the products by the gas chromatograph, and possible small leakage in the reactor system. However, we need to further optimize the reactor configuration and operation, and experimental conditions to fully exploit the beneficial features of titanium oxide nanotubes as support material for ERC.

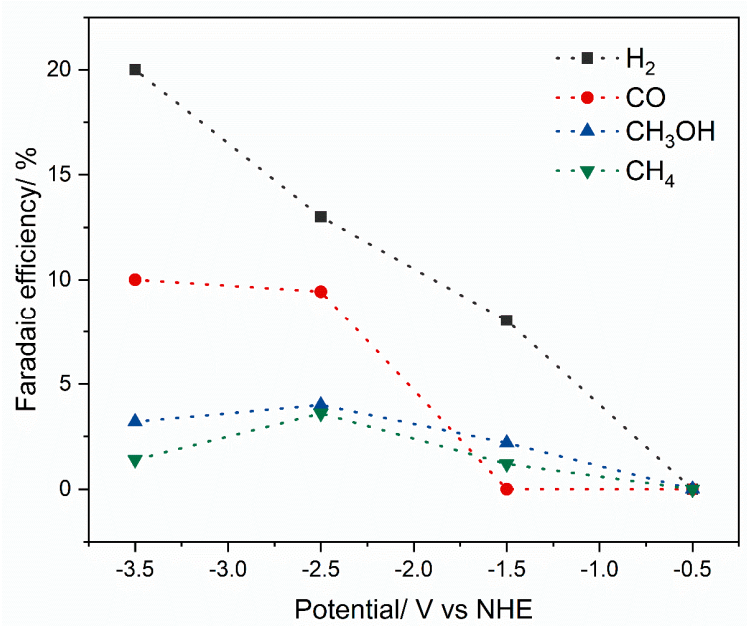

Figure 8. Effect of potential on the product distribution in a solid polymer electrolyte (SPE) reactor.

Table 2. Comparison of the representative research works on supported electrocatalysts for the electrochemical reduction of CO_2.

Catalyst	Catalyst Support	Reaction Medium	Main Products (Faradaic Efficiency, %)	Applied Potential (V)	Reference
Cu/TiO_2 NTs	TiO_2 NTs	Continuous Flow reactor	10% CO, 5% for methanol, with current density of 120 mA/cm^2 36.8% for ethanol	−2.5 V vs. NHE	This work
CuO/TiO_2	TiO_2	Aqueous 0.5 M $KHCO_3$	4.8% Acetone 5.8% n-propanol	0.85 V vs. NHE	Yuan et al. [82]
RuO_2/TiO_2 NTs	TiO_2 NTs	Aqueous 0.5 M $KHCO_3$	60.5% methanol	−0.8 V vs. SCE	Qu et al. [53]
Cu_2O/CNT	CNT	Aqueous 0.5 M $NaHCO_3$	38.0% methanol with current density of 7.5 mA/cm^2	−0.8 V vs. NHE	Malik et al. [83]
SnO_2/MWCNT	MWCNT	Aqueous 0.5 M $NaHCO_3$	27.2% for formate with current density 80 mA/cm^2	−1.7 V vs. SCE	Bashir et al. [74]
Sn/ZSM-5	ZSM-5	Continuous flow reactor	20.6% for methane with current density of 190 mA/cm^2	−2 V vs. NHE	Basu et al. [73]
Ag/C	Carbon	Continuous flow reactor	CO/H_2 (1:2) Total current density of 80 mA/cm^2	−2 V vs. SCE	Delacourt et al. [54]
$Ag//TiO_2$	TiO_2	Continuous Flow reactor	>90%, Partial current density for CO of 101 mA/cm^2	−1.8 vs. Ag/AgCl	Ma et al. [50]

5. Materials and Methods

5.1. Chemicals

Copper nitrate trihydrate, sodium hydroxide, hydrochloric acid, and urea were purchased from Merck®, Darmstadt, Germany. Titanium oxide (Degussa P-25: 75% anatase and 25% rutile) was provided free of cost as a compliment from Cristal Global, Thann, France. Nafion membrane and 5% Nafion solution were purchased from Sigma Aldrich®, St. Louis, MO, USA. Analytical grade sodium bicarbonate was purchased from VWR International, Radnor, PA, USA. High purity (99.99%) nitrogen, argon, and carbon dioxide gases were procured from Abdullah Hashim Gas Co., Jeddah, Saudi Arabia. All chemicals were used as received without any further treatment. Deionized water purified by Millipore® water purification system was used in all experiments.

5.2. Synthesis of Titanium Oxide Nanotubes

The titanium nanotubes were synthesized using a hydrothermal process according to the procedure summarized in the literature [84]. In brief, titanium oxide powder in the mixed anatase and rutile form as Degussa P-25 was used as a starting material. A total of 50 mL of 10 M NaOH was taken in a Teflon beaker and gradually heated until 120 °C. At 120 °C, 2 g of the Degussa powder was added under vigorous mixing. The solution was refluxed at 120 °C for 36 h. The white slurry was treated with 200 mL with 5% HCl solution at 60 °C with stirring, and then washed copiously with deionized water until neutralization. The slurry was air dried at 110 °C for 3 h. The dried powder was calcined in a furnace at 400 °C for 5 h to convert an amorphous phase to well-defined crystallite anatase phase.

5.3. Catalyst Preparation

Copper was loaded on the support material by homogenous precipitation deposition method reported by Cao et al. [85]. Firstly, the calculated amount of preheated Degussa (P-25) was suspended in 200 mL deionized water by sonicating for 30 min. Then, an appropriate amount of copper nitrate was added in the suspension under constant stirring. For example, to achieve 5% copper loading in the final catalysts, 232.8 mg of copper nitrate hexahydrate was added to 950 mg of the support material. The suspension was further stirred and sonicated for one hour to completely dissolve the copper nitrate salt to make a homogenous suspension. The resulting suspension was heated under vigorous stirring until the suspension temperature reaches 90 °C. To this suspension, 30 mL of 0.42 M aqueous urea solution was added drop by drop. The suspension was maintained at 90 °C with vigorous stirring for deposition to take place. At 90 °C, hydrolysis of urea takes place at a reasonable rate so the hydroxyl ions react metal ion resulting in the precipitation as the metal hydroxide. After allowing precipitation-deposition for about 8 h, the slurry was cooled to room temperature, centrifuged, thoroughly washed with deionized water, and dried at 110 °C for 5 h. The powder was calcined at 450 °C in argon flow in a tubular furnace. The calcined samples were finally reduced at 450 °C in 100 mL/min 10% H_2/Ar flow for 4 h. This method was repeated with different amount of the copper nitrate for synthesizing catalysts with 5%, 10%, and 20% by weight copper loading.

5.4. Physical Characterization

X-ray diffraction was performed to identify the crystalline phases and to determine the size of the Cu particles. The XRD profiles were recorded by using a diffractometer (Rigaku D/MAX-IIIA, 3 kW) for 2θ between 20° and 80°.

Field emission scanning electron microscope equipped with energy dispersive X-ray spectroscopy (FESEM) (JEOL JSM-6460LV) and high-resolution transmission electron microscopy (HRTEM) (JEOL-JEM-2100F) were used to investigate the morphology, microstructure, and composition. Nitrogen adsorption and desorption studies were carried out to calculate the surface area, pore volume, and average pore diameter using liquid nitrogen temperature at 77 K using Micromeritics model ASAP-2010.

6. Electrochemical Analysis

6.1. Half Cell

Catalytic activities of the as-prepared catalysts were determined by linear sweep voltammetry (LSV) and chronoamperometry (CA). Electrochemical studies were carried out in a conventional indigenously made H-type cell (0.5 dm^3) with anode and cathode compartments separated by a proton conducting Nafion-117® membrane (Figure 9). The compartments were separated to prevent the cathode and anode products being mixed. Catalyst ink prepared by ultrasonicating 80 mg of the prepared catalysts along with iso-propanol and 0.82 mL of 5% Nafion solution for 30 min. The catalyst ink was then brush-painted on Toray® carbon paper. The catalyst coated (or uncoated) carbon paper and platinum mesh were used as working electrode and counter electrode, respectively. Active surface area of the working electrode and counter electrode were 1.0 and 8.0 cm^2, respectively. Standard calomel electrode (SCE) was used as the reference electrode in all the experiments. A 0.5 molar aqueous solution of sodium bicarbonate was used both as catholyte and anolyte. Firstly, the catholyte solution was purged with high purity nitrogen for 30 min at 50 mL/min and, then with high-purity carbon dioxide at 100 mL/min for 1 h. The pH before and after CO_2 purging was measured to be 8.67 and 7.38, respectively. Linear sweep voltammetry was carried out from 0 to −3 V with scan rate of 25 mV/s and chronoamperometry at −1.7 V for 6000 s. All electrochemical experiments were performed with Autolab PGSTAT 302 potentiostat/galvanostat (Metrohm, Herisau, Switzerland) equipped with Nova® software.

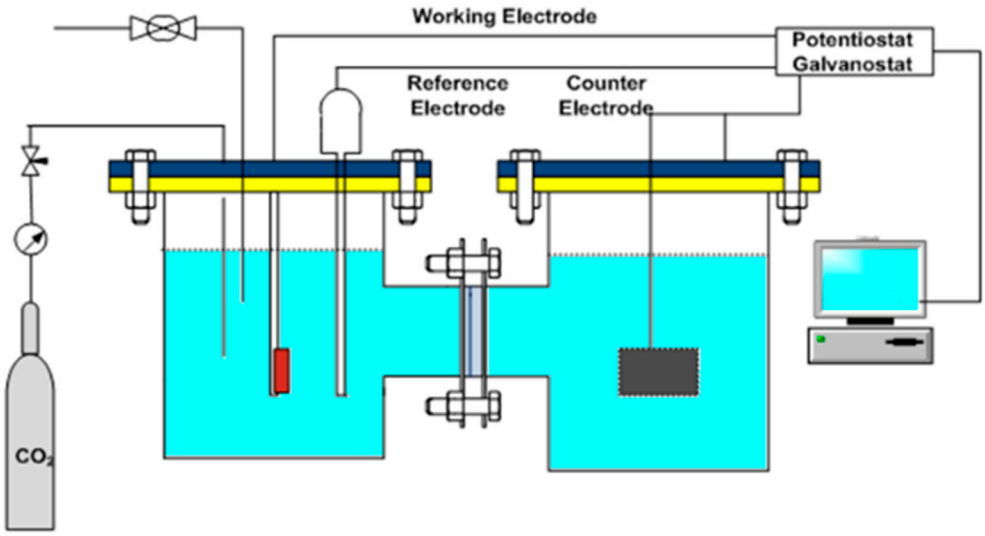

Figure 9. Schematic diagram of half-cell assembly.

6.2. Continuous Solid Polymer Electrolyte Membrane (SPE) Reactor

The continuous electrochemical reactor setup used in this study is shown in Figure S1 (Supplementary Materials). Carbon dioxide was passed through a hydrocarbon trap to remove any trace hydrocarbon present in the reactant gas stream. The flow rate of the gas was 20 mL/min. Gas flow was controlled by a mass flow controller. The tubing for the line is 1/4 inch (63.5 mm). Then, a dewpoint humidifier with gas heating was installed in the line to humidify the CO_2 gas flow. A hygrometer was installed in the line to measure the moisture content and temperature of the gas stream. This humidified CO_2 gas was fed to the cathode side of the cell. The issuing gas from the reactor was first passed through a water trap to remove any moisture. In between the backpressure regulator and electrochemical cell, a sampling point for gas chromatography was provided by a ball valve. Another flow loop was to use a water tank of 5 L and a peristaltic pump was used to deliver water to the anode of the sides of the electrochemical reactor. The electrochemical reactor cell was

similar to systems that are used for fuel-cell studies [54]. The cell was composed of two blocks in which channels were machined and were used as current collectors as well as to feed gaseous (humidified carbon dioxide) or liquid (water) reactants to the cathode and anode respectively. The cathode block was made of graphite treated to make it nonporous. As it can be anticipated that graphite will be oxidized upon electrolysis at the anode, polytetrafluoroethylene (PTFE) was chosen as a material for the anode block. The flow pattern was the same as that in the fuel cell. A platinum screen placed between the PTFE block and the electrode was used as current collector. It was connected to the external circuit by means of a platinum wire through the PTFE block. The membrane-electrode assembly (MEA) was placed between the two blocks. The active area for the cell was 25 cm^2. The whole sandwich was placed between two aluminum/stainless steel frames with eight bolts of diameter (1/4 inch) 0.635 cm fastened. Two stainless-steel plates or aluminum plates (15 cm × 10 cm × 2 cm) were used as back plates to provide mechanical strength and just like fuel cells, the anode and cathode had channels for reactants and products. The product from the cathode compartment was analyzed using an Agilent 7890A gas chromatograph (Agilent Technologies, Santa Clara, CA, USA) equipped with thermal conductivity (TCD) and flame ionization detectors (FID). In short, this was essentially fuel cell hardware with PTFE anode. All other features were kept unchanged.

7. Conclusions

Titanium oxide nanotubes are synthesized using the alkaline hydrothermal method and used as support material for electrocatalyst for the electrochemical reduction of CO_2. It is clear from the characterization results that titanium oxide nanotubes (diameter 2–4 nm) with the exceptionally high surface area (395 m^2/g) are produced by the alkaline hydrothermal process. Nanosized copper particles are successfully deposited on the high surface area support material. The LSV and chronoamperometry results show that all the prepared catalysts effectively reduced CO_2 in aqueous 0.5 $NaHCO_3$ solution, while catalyst with 10% Cu loading showed the highest current density. Methanol was detected in the liquid phase. It is speculated that 10% Cu loading provides a percolation limit for the TNT support and the further increase in loading severely reduced the surface area and pore size of the catalysts. Methanol, methane, CO, and hydrogen are detected as a product in continuous SPE reactor with the optimum catalyst (10% Cu/NT). The faradaic efficiency for methanol, methane, and CO are found to be 4%, 3%, and 10%, respectively, at −2.5 V.

Supplementary Materials: The following are available online at http://www.mdpi.com/2073-4344/9/3/298/s1.

Author Contributions: Conceptualization, S.S.H., S.U.R.; Catalyst synthesis and Characterization, S.S.H. and C.K.C.; Data Analysis, S.S.H. & S.M.J.Z., Supervision, S.U.R., S.M.J.Z.; Writing original draft: S.S.H., J.S.; Writing-review & editing, J.S., G.M. and S.S.H.

Funding: This research work was supported by the Deanship of Scientific Research, King Faisal University, Kingdom of Saudi Arabia, through Nasher Research Project No. 186074.

Acknowledgments: We are grateful to anonymous reviewers for their constructive comments to improve the paper.

Conflicts of Interest: The authors declare no conflict of interest.

References

1. Fleming, R.J. An updated review about carbon dioxide and climate change. *Environ. Earth Sci.* **2018**, *77*, 262. [CrossRef]
2. Florides, G.A.; Christodoulides, P. Global warming and carbon dioxide through sciences. *Environ. Int.* **2009**, *35*, 390–401. [CrossRef] [PubMed]
3. Aresta, M.; Dibenedetto, A. Utilisation of CO_2 as a chemical feedstock: Opportunities and challenges. *Dalton Trans.* **2007**, 2975–2992. [CrossRef] [PubMed]
4. Ball, M.; Wietschel, M. The future of hydrogen-Opportunities and challenges. *Int. J. Hydrog. Energy* **2009**, *34*, 615–627. [CrossRef]

5. Khezri, B.; Fisher, A.C.; Pumera, M. CO_2 reduction: The quest for electrocatalytic materials. *J. Mater. Chem. A* **2017**, *5*, 8230–8246. [CrossRef]
6. Mohammed, Y.S.; Mustafa, M.W.; Bashir, N. Status of renewable energy consumption and developmental challenges in Sub-Sahara Africa. *Renew. Sustain. Energy Rev.* **2013**, *27*, 453–463. [CrossRef]
7. Hossain, S.K.S.; Hoque, M.E. 9—Polymer nanocomposite materials in energy storage: Properties and applications. In *Polymer-Based Nanocomposites for Energy and Environmental Applications*; Jawaid, M., Khan, M.M., Eds.; Woodhead Publishing: Cambridge, MA, USA, 2018; pp. 239–282.
8. Liu, J.; Wang, J.; Xu, C.; Jiang, H.; Li, C.; Zhang, L.; Lin, J.; Shen, Z.X. Advanced Energy Storage Devices: Basic Principles, Analytical Methods, and Rational Materials Design. *Adv. Sci.* **2018**, *5*, 1700322. [CrossRef]
9. Centi, G.; Perathoner, S. Opportunities and prospects in the chemical recycling of carbon dioxide to fuels. *Catal. Today* **2009**, *148*, 191–205. [CrossRef]
10. Rahman, S.U.; Zaidi, S.M.J.; Ahmed, S.; Hossain, S.S. Electrocatalyst for Electrochemical Conversion of Carbon Dioxide. U.S. Patent US9109293B2, 18 August 2015.
11. Fu, Y.; Yang, H.; Du, R.; Tu, G.; Xu, C.; Zhang, F.; Fan, M.; Zhu, W. Enhanced photocatalytic CO_2 reduction over Co-doped NH2-MIL-125(Ti) under visible light. *RSC Adv.* **2017**, *7*, 42819–42825. [CrossRef]
12. Zhang, W.; Hu, Y.; Ma, L.; Zhu, G.; Wang, Y.; Xue, X.; Chen, R.; Yang, S.; Jin, Z. Progress and Perspective of Electrocatalytic CO_2 Reduction for Renewable Carbonaceous Fuels and Chemicals. *Adv. Sci.* **2018**, *5*, 1700275. [CrossRef]
13. DuBois, D.L. *Electrochemical Reactions of Carbon Dioxide*; Wiley-VCH Verlag GmbH & Co. KGaA: Weinheim, Germany, 2007. [CrossRef]
14. Wu, H.; Song, J.; Xie, C.; Hu, Y.; Han, B. Highly efficient electrochemical reduction of CO_2 into formic acid over lead dioxide in an ionic liquid–catholyte mixture. *Green Chem.* **2018**, *20*, 1765–1769. [CrossRef]
15. Olajire, A.A. Recent progress on the nanoparticles-assisted greenhouse carbon dioxide conversion processes. *J. CO_2 Util.* **2018**, *24*, 522–547. [CrossRef]
16. Qiao, J.; Liu, Y.; Hong, F.; Zhang, J. A review of catalysts for the electroreduction of carbon dioxide to produce low-carbon fuels. *Chem. Soc. Rev.* **2014**, *43*, 631–675. [CrossRef] [PubMed]
17. Lim, R.J.; Xie, M.; Sk, M.A.; Lee, J.-M.; Fisher, A.; Wang, X.; Lim, K.H. A review on the electrochemical reduction of CO_2 in fuel cells, metal electrodes and molecular catalysts. *Catal. Today* **2014**, *233*, 169–180. [CrossRef]
18. Leung, D.Y.C.; Caramanna, G.; Maroto-Valer, M.M. An overview of current status of carbon dioxide capture and storage technologies. *Renew. Sustain. Energy Rev.* **2014**, *39*, 426–443. [CrossRef]
19. Al-Rowaili, F.N.; Jamal, A.; Ba Shammakh, M.S.; Rana, A. A Review on Recent Advances for Electrochemical Reduction of Carbon Dioxide to Methanol Using Metal–Organic Framework (MOF) and Non-MOF Catalysts: Challenges and Future Prospects. *ACS Sustain. Chem. Eng.* **2018**, *6*, 15895–15914. [CrossRef]
20. Zhao, G.; Huang, X.; Wang, X.; Wang, X. Progress in catalyst exploration for heterogeneous CO_2 reduction and utilization: A critical review. *J. Mater. Chem. A* **2017**, *5*, 21625–21649. [CrossRef]
21. Hori, Y.; Ketshuei, K.; Murata, A.; Suzuki, S. Production of methane and ethylene in Electrochemical reduction of carbon dioxide in the aqueous hydrogen carbonate solution. *Chem. Lett.* **1986**, *15*, 897–898. [CrossRef]
22. Gong, J.; Zhang, L.; Zhao, Z.-J. Nanostructured Materials for Heterogeneous Electrocatalytic CO_2 Reduction and Related Reaction Mechanisms. *Angew. Chem. Int. Ed.* **2017**. [CrossRef]
23. Centi, G.; Perathoner, S.; Wine, G.; Gangeri, M. Electrocatalytic conversion of CO_2 to long carbon-chain hydrocarbons. *Green Chem.* **2007**, *9*, 671–678. [CrossRef]
24. Gattrell, M.; Gupta, N.; Co, A. A review of the aqueous electrochemical reduction of CO_2 to hydrocarbons at copper. *J. Electroanal. Chem.* **2006**, *594*, 1–19. [CrossRef]
25. Luo, W.; Nie, X.; Janik, M.J.; Asthagiri, A. Facet Dependence of CO_2 Reduction Paths on Cu Electrodes. *ACS Catal.* **2016**, *6*, 219–229. [CrossRef]
26. Garg, G.; Basu, S. Studies on Degradation of Copper Nano Particles in Cathode for CO_2 Electrolysis to Organic Compounds. *Electrochim. Acta* **2015**, *177*, 359–365. [CrossRef]
27. Qiao, J.; Jiang, P.; Liu, J.; Zhang, J. Formation of Cu nanostructured electrode surfaces by an annealing–electroreduction procedure to achieve high-efficiency CO_2 electroreduction. *Electrochem. Commun.* **2014**, *38*, 8–11. [CrossRef]

28. Hori, Y.; Murata, A.; Takahashi, R. Formation of Hydrocarbons in the Electrochemical Reduction of Carbon Dioxide at a Copper Electrode in Aqueous Solution. *J. Chem. Soc. Faraday Trans. 1 Phys. Chem. Condens. Phases* **1989**, *85*, 2309–2326. [CrossRef]
29. Kaneco, S.; Iiba, K.; Ohta, K.; Mizuno, T. Electrochemical reduction of carbon dioxide on copper in methanol with various potassium supporting electrolytes at low temperature. *J. Solid State Electrochem.* **1999**, *3*, 424–428.
30. Kaneco, S.; Ueno, Y.; Katsumata, H.; Suzuki, T.; Ohta, K. Electrochemical reduction of CO_2 in copper particle-suspended methanol. *Chem. Eng. J.* **2006**, *119*, 107–112. [CrossRef]
31. Frese, K.W. Electrochemical reduction of CO_2 at intentionally oxidezed copper electrodes. *J. Ectrochem. Soc.* **1991**, *138*, 3338–3344. [CrossRef]
32. Ohya, S.; Kaneco, S.; Katsumata, H.; Suzuki, T.; Ohta, K. Electrochemical reduction of CO_2 in methanol with aid of CuO and Cu_2O. *Catal. Today* **2009**, *148*, 329–334. [CrossRef]
33. Chang, T.-Y.; Liang, R.-M.; Wu, P.-W.; Chen, J.-Y.; Hsieh, Y.-C. Electrochemical reduction of CO_2 by Cu_2O-catalyzed carbon clothes. *Mater. Lett.* **2009**, *63*, 1001–1003. [CrossRef]
34. Le, M.; Ren, M.; Zhang, Z.; Sprunger, P.T.; Kurtz, R.L.; Flake, J.C. Electrochemical Reduction of CO_2 to CH_3OH at Copper Oxide Surfaces. *J. Electrochem. Soc.* **2011**, *158*, E45–E49. [CrossRef]
35. Roberts, F.S.; Kuhl, K.P.; Nilsson, A. High Selectivity for Ethylene from Carbon Dioxide Reduction over Copper Nanocube Electrocatalysts. *Angew. Chem. Int. Ed.* **2015**, *54*, 5179–5182. [CrossRef] [PubMed]
36. Yamamoto, T.; Tryk, D.A.; Hashimoto, K.; Fujishima, A.; Okawa, M. Electrochemical Reduction of CO_2 in the Micropores of Activated Carbon Fibers. *J. Electrochem. Soc.* **2000**, *147*, 3393–4000. [CrossRef]
37. Bashir, S.M.; Hossain, S.S.; ur Rahman, S.; Ahmed, S.; Hossain, M.M. NiO/MWCNT Catalysts for Electrochemical Reduction of CO_2. *Electrocatalysis* **2015**, *6*, 544–553. [CrossRef]
38. Safdar Hossain, S.; Rahman, S.u.; Ahmed, S. Electrochemical Reduction of Carbon Dioxide over CNT-Supported Nanoscale Copper Electrocatalysts. *J. Nanomater.* **2014**, *2014*, 10. [CrossRef]
39. He, H.; Jagvaral, Y. Electrochemical reduction of CO_2 on graphene supported transition metals—Towards single atom catalysts. *Phys. Chem. Chem. Phys.* **2017**, *19*, 11436–11446. [CrossRef] [PubMed]
40. Kornienko, N.; Zhao, Y.; Kley, C.S.; Zhu, C.; Kim, D.; Lin, S.; Chang, C.J.; Yaghi, O.M.; Yang, P. Metal–Organic Frameworks for Electrocatalytic Reduction of Carbon Dioxide. *J. Am. Chem. Soc.* **2015**, *137*, 14129–14135. [CrossRef]
41. Daiyan, R.; Tan, X.; Chen, R.; Saputera, W.H.; Tahini, H.A.; Lovell, E.; Ng, Y.H.; Smith, S.C.; Dai, L.; Lu, X.; et al. Electroreduction of CO_2 to CO on a Mesoporous Carbon Catalyst with Progressively Removed Nitrogen Moieties. *ACS Energy Lett.* **2018**, *3*, 2292–2298. [CrossRef]
42. Engl, T.; Gubler, L.; Schmidt, T.J. Fuel Electrode Carbon Corrosion in High Temperature Polymer Electrolyte Fuel Cells—Crucial or Irrelevant? *Energy Technol.* **2016**, *4*, 65–74. [CrossRef]
43. Roy, P.; Berger, S.; Schmuki, P. TiO_2 Nanotubes: Synthesis and Applications. *Angew. Chem. Int. Ed.* **2011**, *50*, 2904–2939. [CrossRef]
44. Liu, N.; Chen, X.; Zhang, J.; Schwank, J.W. A review on TiO_2-based nanotubes synthesized via hydrothermal method: Formation mechanism, structure modification, and photocatalytic applications. *Catal. Today* **2014**, *225*, 34–51. [CrossRef]
45. Balčiūnaitė, A.; Tamašauskaitė-Tamašiūnaitė, L.; Santos, D.M.F.; Zabielaitė, A.; Jagminienė, A.; Stankevičienė, I.; Norkus, E. Au Nanoparticles Modified Co/Titania Nanotubes as Electrocatalysts for Borohydride Oxidation. *Fuel Cells* **2017**, *17*, 690–697. [CrossRef]
46. Zhang, J.; Su, N.; Hu, X.; Zhu, F.; Yu, Y.; Yang, H. Facile synthesis of Pt nanoparticles supported on anatase TiO_2 nanotubes with good photo-electrocatalysis performance for methanol. *RSC Adv.* **2017**, *7*, 56194–56203. [CrossRef]
47. Abdullah, M.; Kamarudin, S.K.; Shyuan, L.K. TiO_2 Nanotube-Carbon (TNT-C) as Support for Pt-based Catalyst for High Methanol Oxidation Reaction in Direct Methanol Fuel Cell. *Nanoscale Res. Lett.* **2016**, *11*, 553. [CrossRef] [PubMed]
48. Abraham, B.G.; Maniam, K.K.; Kuniyil, A.; Chetty, R. Electrocatalytic Performance of Palladium Dendrites Deposited on Titania Nanotubes for Formic Acid Oxidation. *Fuel Cells* **2016**, *16*, 656–661. [CrossRef]
49. Cueto-Gómez, L.F.; Garcia-Gómez, N.A.; Mosqueda, H.A.; Sánchez, E.M. Electrochemical study of TiO_2 modified with silver nanoparticles upon CO_2 reduction. *J. Appl. Electrochem.* **2014**, *44*, 675–682. [CrossRef]
50. Ma , S.; Lan , Y.; Perez, G.M.J.; Moniri, S.; Kenis , P.J.A. Silver Supported on Titania as an Active Catalyst for Electrochemical Carbon Dioxide Reduction. *ChemSusChem* **2014**, *7*, 866–874. [CrossRef]

51. Yuan, J.; Liu, L.; Guo, R.-R.; Zeng, S.; Wang, H.; Lu, J.-X. Electroreduction of CO_2 into Ethanol over an Active Catalyst: Copper Supported on Titania. *Catalysts* **2017**, *7*, 220. [CrossRef]
52. Yuan, J.; Yang, M.-P.; Hu, Q.-L.; Li, S.-M.; Wang, H.; Lu, J.-X. Cu/TiO_2 nanoparticles modified nitrogen-doped graphene as a highly efficient catalyst for the selective electroreduction of CO_2 to different alcohols. *J. CO_2 Util.* **2018**, *24*, 334–340. [CrossRef]
53. Qu, J.; Zhang, X.; Wang, Y.; Xie, C. Electrochemical reduction of CO_2 on RuO_2/TiO_2 nanotubes composite modified Pt electrode. *Electrochim. Acta* **2005**, *50*, 3576–3580. [CrossRef]
54. Delacourt, C.; Ridgway, L.P.; John, B.K.; Newman, J. Design of an Electrochemical Cell Making Syngas (CO + H_2) from CO_2 and H_2O Reduction at Room Temperature. *J. Electrochem. Soc.* **2008**, *155*, B42–B49. [CrossRef]
55. Burdyny, T.; Smith, W.A. CO_2 reduction on gas-diffusion electrodes and why catalytic performance must be assessed at commercially-relevant conditions. *Energy Environ. Sci.* **2019**. [CrossRef]
56. Dewulf, D.W.; Bard, A.J. The electrochemical reduction of CO_2 to CH_4 and C_2H_4 at Cu/Nafion electrodes (solid polymer electrolyte structures). *Catal. Lett.* **1988**, *1*, 73–79. [CrossRef]
57. Komatsu, S.; Tanaka, M.; Okumura, A.; Kungi, A. Preparation of cu-solid polymer electrolyte composite electrodes and application to gas-phase electrochemical reduction of CO_2. *Electrochim. Acta* **1995**, *40*, 745–753. [CrossRef]
58. Ma, L.; Fan, S.; Zhen, D.; Wu, X.; Liu, S.; Lin, J.; Huang, S.; Chen, W.; He, G. Electrochemical Reduction of CO_2 in Proton Exchange Membrane Reactor: The Function of Buffer Layer. *Ind. Eng. Chem. Res.* **2017**, *56*, 10242–10250. [CrossRef]
59. Sun, K.C.; Qadir, M.B.; Jeong, S.H. Hydrothermal synthesis of TiO_2 nanotubes and their application as an over-layer for dye-sensitized solar cells. *RSC Adv.* **2014**, *4*, 23223–23230. [CrossRef]
60. Cao, J.-L.; Yan, Z.-L.; Deng, Q.-F.; Yuan, Z.-Y.; Wang, Y.; Sun, G.; Wang, X.-D.; Hari, B.; Zhang, Z.-Y. Homogeneous precipitation method preparation of modified red mud supported Ni mesoporous catalysts for ammonia decomposition. *Catal. Sci. Technol.* **2014**, *4*, 361–368. [CrossRef]
61. Li, W.; Liang, R.; Hu, A.; Huang, Z.; Zhou, Y.N. Generation of oxygen vacancies in visible light activated one-dimensional iodine TiO_2 photocatalysts. *RSC Adv.* **2014**, *4*, 36959–36966. [CrossRef]
62. Lee, K.; Mazare, A.; Schmuki, P. One-Dimensional Titanium Dioxide Nanomaterials: Nanotubes. *Chem. Rev.* **2014**, *114*, 9385–9454. [CrossRef]
63. Kasuga, T.; Hiramatsu, M.; Hoson, A.; Sekino, T.; Niihara, K. Titania Nanotubes Prepared by Chemical Processing. *Adv. Mater.* **1999**, *11*, 1307–1311. [CrossRef]
64. Mortada, W.I.; Moustafa, A.F.; Ismail, A.M.; Hassanien, M.M.; Aboud, A.A. Microwave assisted decoration of titanium oxide nanotubes with $CuFe_2O_4$ quantum dots for solid phase extraction of uranium. *RSC Adv.* **2015**, *5*, 62414–62423. [CrossRef]
65. Li, W.; Fu, T.; Xie, F.; Yu, S.; He, S. The multi-staged formation process of titanium oxide nanotubes and its thermal stability. *Mater. Lett.* **2007**, *61*, 730–735. [CrossRef]
66. Chen, S.-A.; Nian, J.-N.; Tsai, C.-C.; Teng, H. TiO_2 Nanotube-Supported Cu as the Catalyst for Selective NO Reduction with NH3. *J. Air Waste Manag. Assoc.* **2007**, *57*, 600–605. [CrossRef] [PubMed]
67. Rahmatolahzadeh, R.; Ebadi, M.; Motevalli, K. Preparation and characterization of Cu clusters and Cu–Ag alloy via galvanic replacement method for azo dyes degradation. *J. Mater. Sci. Mater. Electron.* **2017**, 1–8. [CrossRef]
68. Huang, C.; Long, Z.; Miyauchi, M.; Qiu, X. A facile one-pot synthesis of Cu-Cu_2O concave cube hybrid architectures. *CrystEngComm* **2014**, *16*, 4967–4972. [CrossRef]
69. Pappas, D.K.; Boningari, T.; Boolchand, P.; Smirniotis, P.G. Novel manganese oxide confined interweaved titania nanotubes for the low-temperature Selective Catalytic Reduction (SCR) of NOx by NH3. *J. Catal.* **2016**, *334*, 1–13. [CrossRef]
70. Kasuga, T.; Hiramatsu, M.; Hoson, A.; Sekino, T.; Niihara, K. Formation of Titanium Oxide Nanotube. *Langmuir* **1998**, *14*, 3160–3163. [CrossRef]
71. Hernandez, R.M.; Marquez, J.; Marquez, O.P.; Choy, M.; Ovalles, C.; Garcia, J.J.; Scharifker, B. Reduction of Carbon Dioxide on Modified Glassy Carbon Electrodes. *J. Electrochem. Soc.* **1999**, *146*, 4131–4136. [CrossRef]
72. Rasul, S.; Pugnant, A.; Yu, E. Electrochemical Reduction of CO_2 at Multi-Metallic Interfaces. *ECS Trans.* **2018**, *85*, 57–66. [CrossRef]
73. Liu, X.; Zhu, L.; Wang, H.; He, G.; Bian, Z. Catalysis performance comparison for electrochemical reduction of CO2 on Pd–Cu/graphene catalyst. *RSC Adv.* **2016**, *6*, 38380–38387. [CrossRef]

74. Bhattacharyya, K.; Danon, A.; Vijayan, B.K.; Gray, K.A.; Stair, P.C.; Weitz, E. Role of the Surface Lewis Acid and Base Sites in the Adsorption of CO_2 on Titania Nanotubes and Platinized Titania Nanotubes: An in Situ FT-IR Study. *J. Phys. Chem. C* **2013**, *117*, 12661–12678. [CrossRef]
75. Basu, S.; Shegokar, A.; Biswal, D. Synthesis and characterization of supported Sn/γ-Al_2O_3 and Sn/ZSM5 catalysts for CO_2 reduction in electrochemical cell. *J. CO_2 Util.* **2017**, *18*, 80–88. [CrossRef]
76. Bashir, S.; Hossain, S.S.; Rahman, S.U.; Ahmed, S.; Amir, A.-A.; Hossain, M.M. Electrocatalytic reduction of carbon dioxide on SnO2/MWCNT in aqueous electrolyte solution. *J. CO_2 Util.* **2016**, *16*, 346–353. [CrossRef]
77. Spataru, N.; Tokuhiro, K.; Terashima, C.; Rao, T.N.; Fujishima, A. Electrochemical reduction of carbon dioxide at ruthenium dioxide deposited on boron-doped diamond. *J. Appl. Electrochem.* **2003**, *33*, 1205–1210. [CrossRef]
78. Chaplin, R.P.S.; Wragg, A.A. Effects of process conditions and electrode material on reaction pathways for carbon dioxide electroreduction with particular reference to formate formation. *J. Appl. Electrochem.* **2003**, *33*, 1107–1123. [CrossRef]
79. Kaneco, S.; Iiba, K.; Hiei, N.-H.; Ohta, K.; Mizuno, T.; Suzuki, T. Electrochemical reduction of carbon dioxide to ethylene with high Faradaic efficiency at a Cu electrode in CsOH/methanol. *Electrochim. Acta* **1999**, *44*, 4701–4706. [CrossRef]
80. Kaneco, S.; Iiba, K.; Katsumata, H.; Suzuki, T.; Ohta, K. Effect of sodium cation on the electrochemical reduction of CO_2 at a copper electrode in methanol. *J. Solid State Electrochem.* **2007**, *11*, 490–495. [CrossRef]
81. Koleli, F.; Balun, D. Reduction of CO_2 under high pressure and high temperature on Pb-granule electrodes in a fixed-bed reactor in aqueous medium. *Appl. Catal. A Gen.* **2004**, *274*, 237–242. [CrossRef]
82. Yamamoto, T.; Tryk, D.A.; Fujishima, A.; Ohata, H. Production of syngas plus oxygen from CO_2 in a gas-diffusion electrode-based electrolytic cell. *Electrochim. Acta* **2002**, *47*, 3327–3334. [CrossRef]
83. Kuhl, K.P.; Cave, E.R.; Abram, D.N.; Jaramillo, T.F. New insights into the electrochemical reduction of carbon dioxide on metallic copper surfaces. *Energy Environ. Sci.* **2012**, *5*, 7050–7059. [CrossRef]
84. Yuan, J.; Zhang, J.-J.; Yang, M.-P.; Meng, W.-J.; Wang, H.; Lu, J.-X. CuO Nanoparticles Supported on TiO_2 with High Efficiency for CO_2 Electrochemical Reduction to Ethanol. *Catalysts* **2018**, *8*, 171. [CrossRef]
85. Irfan Malik, M.; Malaibari, Z.O.; Atieh, M.; Abussaud, B. Electrochemical reduction of CO_2 to methanol over MWCNTs impregnated with Cu_2O. *Chem. Eng. Sci.* **2016**, *152*, 468–477. [CrossRef]